Deep Cavitand Self-Assembled on Au NPs-MWCNT as Highly Sensitive Benzene Sensing Interface

Pierrick Clément, Saša Korom, Claudia Struzzi, Enrique J. Parra, Carla Bittencourt, Pablo Ballester, and Eduard Llobet**

The unprecedented sensitivity and partial selectivity of quinoxaline-walled thioether-legged deep cavitand functionalized multiwall carbon nanotubes toward traces of benzene vapors are presented. The cavitand is grafted onto gold nanoparticle (Au-NP) decorated oxygen plasma treated multiwall carbon nanotubes (O-MWCNT) by a self-assembled monolayer process affording a product referred to as cav-Au-MWCNT. The reported technique is suitable for the mass production of hybrid nanomaterials at low cost. The cav-Au-MWCNT resistive gas sensor operates at room temperature and shows an outstanding performance toward traces of benzene vapors. The detection of 2.5 ppb of benzene in dry air is demonstrated with a limit of detection (LOD) near 600 ppt. For the first time, it is shown that a CNT nanomaterial can effectively sense the extremely harmful benzene molecule with higher sensitivity than toluene or *o*-xylene at the trace levels. The cavitand is well suited for binding benzene, which, being in close proximity to the MWCNT, affects its density of states (DOS) shifting the Fermi level away from the valence band. The binding of benzene is transduced in a diminution of MWCNT conductance. Furthermore, the inclusion of benzene is fully reversible at room temperature, implying that the sensor can operate at very low power consumption.

1. Introduction

Benzene is a nonpolar six-membered ring aromatic hydrocarbon with molecular formula C_6H_6, with dimensions of ≈6.0 × 3.5 Å and a volume of 120 Å^3. It belongs to the BTEX (benzene, toluene, ethylbenzene, and xylene) group of compounds. The components of this group feature similar structures but quite different toxicological properties. Benzene is listed among the most harmful volatile organic compounds (VOC). It has highly flammable and toxic vapors and is recognized as a human carcinogen by the US Environmental Protection Agency and the European Commission.[1] Long-term exposures to relatively low concentrations of benzene over months or years lead to severe hemotoxic effects such as aplastic anemia and pancytopenia and to acute nonlymphocytic leukemia.[2] In the last 10 years, the permissible exposure limit has been lowered from 10 ppm to 100 ppb.[3] According to the Directive 2008/50/EC of the European Parliament and of the Council of May 2008, the limit value for the annual average exposure to benzene is 5 µg m^{-3} (1.6 ppb).[4]

Nowadays, several methods for detecting benzene traces are in use. Most of them involve pumping of the sample and subsequent analysis by employing colorimetric detector tubes or gas chromatography (GC-FID, GC-MS). These methods are bulky, expensive, and do not allow implementation for a continuous monitoring of benzene traces. In the last few years, preconcentration methods and GC equipment have been improved in terms of miniaturization and with an LOD reaching the ppb level for benzene.[5] However, such systems are still limited by their long response time, high power consumption, and high cost. Alternatively, the use of portable photoionization detectors (PID) has been reported as well, but PID devices are not selective to benzene and give a total reading for VOCs. The only option to make PID more selective for benzene is to utilize a single-use, disposable, and rather expensive filter at the inlet port of the device that would result in a dramatic cost increase of running benzene measurements. The petrochemical industry, land reclamation, petroleum coke oven operators, petrol stations, motor vehicle repair places, roadside works and many other industries in which their activity may result in exposure to benzene, would clearly benefit from affordable, portable, highly sensitive and selective detectors able to run continuous measurements.

The fact that benzene lacks active chemical functional group(s) renders its trace detection a challenge by employing

P. Clément, Dr. E. J. Parra, Prof. E. Llobet
MINOS-EMaS
Universitat Rovira i Virgili
Avenida Paisos Catalans 26, 43007 Tarragona, Spain
E-mail: eduard.llobet@urv.cat
Dr. S. Korom, Prof. P. Ballester
Institute of Chemical Research of Catalonia (ICIQ)
Av. Països Catalans 16, 43007 Tarragona, Spain
E-mail: pballester@iciq.es
C. Struzzi, Dr. C. Bittencourt
ChIPS
Université de Mons
Place du Parc 23, 7000 Mons, Belgium
Prof. P. Ballester
Catalan Institution for Research and Advanced Studies (ICREA)
Passeig de Lluís Companys, 23
08010 Barcelona, Spain

DOI: 10.1002/adfm.201501234

miniaturized sensors. For a few decades, many studies have been focused on the use of weak and reversible interactions for the development of receptors for the selective complexation of aromatic compounds via "host–guest" strategy. Cram et al. pioneered host–guest studies using deep cavitands derived from resorcin[4]arene scaffolds.[6] The shallow aromatic cavity present in the resorcin[4]arene parent compound was further elaborated by installing bridging groups at the upper rim. Quinoxaline-bridged resorcin[4]arene cavitands are known to bind aromatic guests (e.g., benzene, toluene, fluorobenzene), not only in the liquid, but also in the gas phase.[7] The attractive CH–π and π–π interactions established between the receptor and the included aromatic compound constitute the main driving forces responsible for the formation of inclusion complexes. Thoden et al. modified the alkyl substituents at the lower rim of the cavitands with thioether functions in order to anchor the receptors on a gold surface.[8] The improvements achieved in the synthesis of the cavitands, together with the possibility of depositing them as self-assembled monolayers on different solid substrates, led to the emergence of new strategies in the design of sensors devices.[9] Consequently, several approaches for the detection of aromatic compounds in both liquid and gas phases have been reported. The recognition event (formation of a host–guest complex) was transduced in changes on optical properties (surface plasmon resonance,[10] fluorescence spectroscopy[11]) or in mass changes in the case of resonant devices (quartz crystal micro balance sensor,[12] or a PZT piezoelectric device).[13] For these devices, the reported LOD for BTEX ranges from 50 to hundreds of ppm. Resorcin[4]arene cavitands have also been used as absorbent materials in preconcentrator devices coupled to a μ-GC column for analyte separation. Furthermore, the detection of analytes was performed by a metal oxide gas sensor or mass spectrometer.[14] In these examples, the detection limit for BTEX was found to be in the ppb range.[15] Recently, resorcin[4]arene cavitands were covalently attached to carbon nanotubes (CNTs) that acted as transducers[16] for conductance measurement in the solid–liquid sensor interphase. CNTs have attracted considerable interest as nanomaterial for sensing in solid–gas interphase.[17] They are particularly sensitive to local chemical environment of the gas phase.[18] The functionalization of CNTs with metal–NPs has been exploited to enhance the sensitivity of the material for benzene sensing, reaching an LOD of about 50 ppb in dry air.[19] The metal–NP–CNT system acts as the transduction unit of the adsorption event in a resistive gas sensor. Indeed, the interaction of the material with molecules of benzene in the gas phase results in an electronic charge transfer process between the organic molecule and the metal–NP–CNT nanomaterial. This affects the position of the Fermi energy and, hence, the conductivity of the detection unit. The different used metals show different response toward a variety of gas or vapor molecules, which can be used to improve the selectivity.[20] However, the decoration of CNTs with metal nanoparticles for improving the device's selectivity has been implemented with limited success because these nanomaterials show similar sensitivity to a variety of aromatic compounds and heating is needed to recover the sensor baseline.[19a]

Here, we describe a simple experimental procedure to prepare an unprecedented type of resistive gas sensing device that employs gold nanoparticle (Au-NP) decorated oxygen-functionalized multiwall carbon nanotubes (O-MWCNTs). The Au-NPs are functionalized after deposition on the O-MWCNTs with quinoxaline-walled thioether-legged cavitand **4** (**Figure 1**), leading to highly sensitive molecular recognition of benzene vapors. Additionally, we explored the sensitivity of the sensor toward other air pollutants such as toluene, *o*-xylene, carbon monoxide, nitrogen dioxide, and ethanol vapors in order to evaluate cross sensitivity. The gas sensing mechanism is discussed on the basis of the experimental findings and the mechanism of inclusion complex (benzene $\subset$ **4**) formation in the light of reported, structurally related systems in solutions.

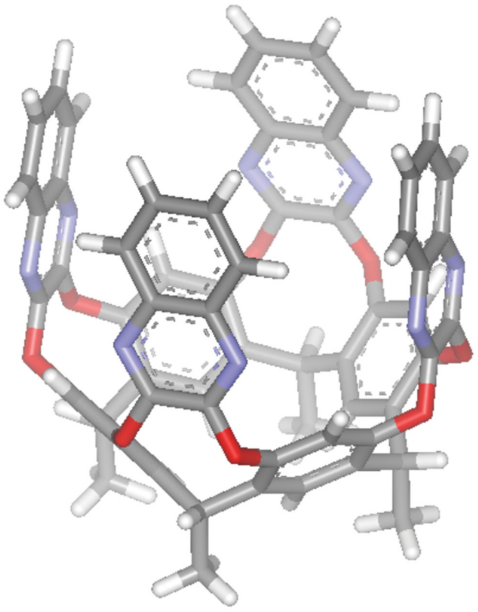

Figure 1. Energy-minimized (MM3 as implemented in Scigress v3.0) structure of cavitand **4** in vase conformation. Included molecule is omitted and cavitand legs —$(CH_2)_9$—S—$(CH_2)_9$—CH_3 are presented as methyl groups for clarity.

2. Results and Discussion

2.1. Anchoring of the Cavitand on MWCNTs

The gas-sensitive, hybrid nanomaterial was prepared by employing a three-step approach. In the first step, MWCNTs were treated with oxygen in plasma to create surface-oxygenated defects quoted in the literature as VO_2 (oxygenated vacancies) and V_2O_2 (oxygenated double-vacancies); these carbon nanotubes are referred to as O-MWCNT.[21] In the second step, the O-MWCNTs were decorated with Au nanoparticles by means of RF sputtering and finally, in the third step, the Au-decorated and oxygen plasma treated MWCNTs (referred to as Au-MWCNT) were functionalized with a self-assembled monolayer of cavitand **4** to produce a desired hybrid material (referred to as cav-Au-MWCNT). These steps are illustrated in **Figure 2**.

The sensing properties of the cav-Au-MWCNTs when operated at room temperature were studied by exposing them to different chemical environments (benzene, toluene, *o*-xylene,

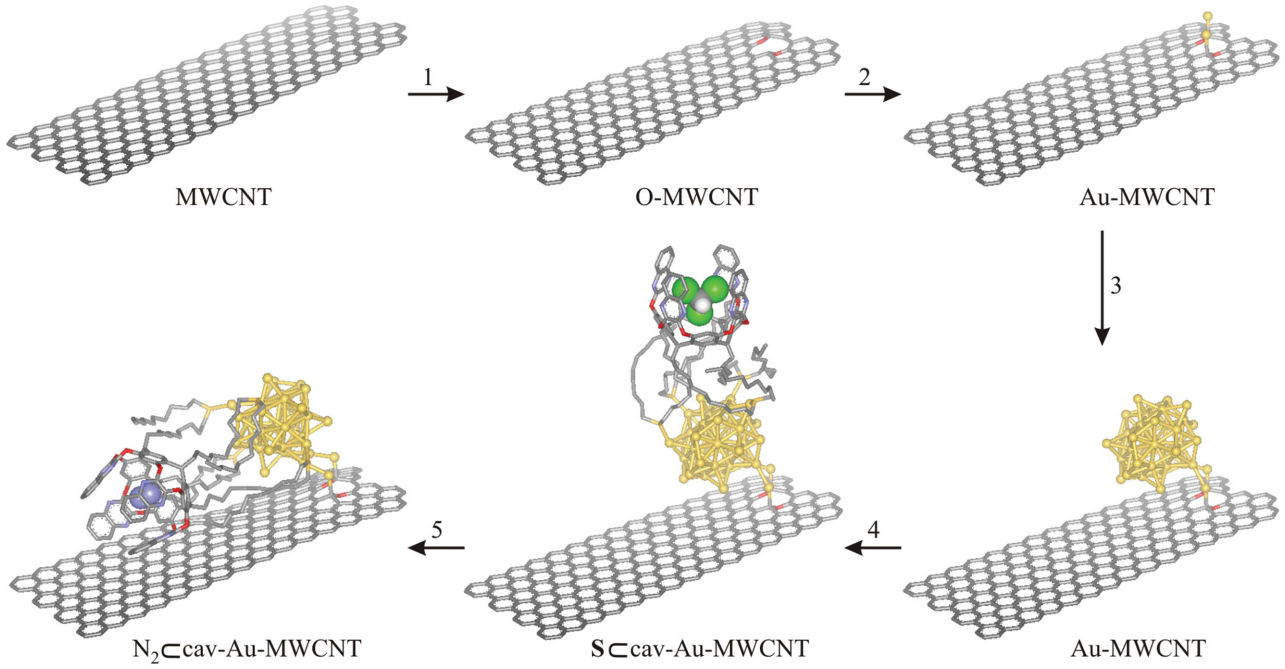

Figure 2. Schematic representation of the preparation of the cav-Au-MWCNT material: 1) oxygen plasma treatment; 2) Au-RF-sputtering (formation of Au-nucleus); 3) Au-RF-sputtering (growth of Au-nucleus and formation of Au-NP); 4) self-assembly of the cavitand **4** monolayer on the Au-NP surface by dipping the material in a chloroform (**S**) solution of the cavitand **4**; 5) solvent removal (an air molecule, e.g., nitrogen, replaces chloroform (**S**) molecule from the cavitand interior).[22] Nitrogen and chloroform molecules are presented as CPK models. Hydrogen atoms are omitted for clarity. Symbol ⊂ stands for "included in." Note: we hypothesize that upon chloroform removal, the cavitand legs are no longer solvated and the molecule collapses on the Au-MWCNT surface.

carbon monoxide, ethanol, and nitrogen dioxide) at different concentrations. For comparison, the results obtained in the gas sensing measurements performed on Au-MWCNT sensors are also reported.

2.2. Step-by-Step Characterization

The morphology and chemical composition of the active layers were characterized using transmission electron microscopy (TEM, **Figures 3** and **4**) and X-ray photoelectron spectroscopy (XPS, **Figure 5**). The homogeneous dispersion of Au nanoparticles (average diameter ≈2 nm) on MWCNTs is illustrated in Figure 3. Figure 4a,b shows that the SAM procedure, implemented for Au-MWCNTs functionalization with the cavitand **4**, promoted aggregation of the previously deposited Au-NPs (with cluster diameters ranging from 10 to 15 nm). The immersion of Au-MWCNTs in a chloroform solution of the cavitand **4** (0.5×10^{-3} M) under mild heating (60 °C), as required by the SAM technique,[17] favored both the cavitand assembly on the Au-NPs and their aggregation on the MWCNTs. We performed XPS analyses for O-MWCNT, Au-MWCNT, cav-Au-MWCNT, and cavitand **4** samples.

In Figure 5a, we show the XPS spectra acquired for (1) O_2 plasma-treated MWCNTs, (2) gold-decorated O-MWCNTs, and (3, 4) cav-Au-MWCNTs samples. The XPS spectra for the cavitand **4** alone (5) are included to assist in the identification of important features in the XPS spectra of cav-Au-MWCNTs samples differing in the time used for the construction of the SAM: 13 h (3) and 24 h (4). All samples contained the oxygen peak corresponding to O_{1s} (Figure 5a) due to the oxygen plasma treatment experienced by the MWCNTs. All Au-decorated samples showed the characteristic Au_{4d} and Au_{4f} doublets. The presence of the cavitand **4** on cav-Au-MWCNT samples, and therefore, the success of the functionalization protocol, was confirmed by the observation of the N_{1s} peak located at 399 eV. This peak is diagnostic of the presence of organic nitrogen and appears only in the spectra of the cavitand and cav-Au-MWCNT samples (Figure 5b). We obtained similar values of relative

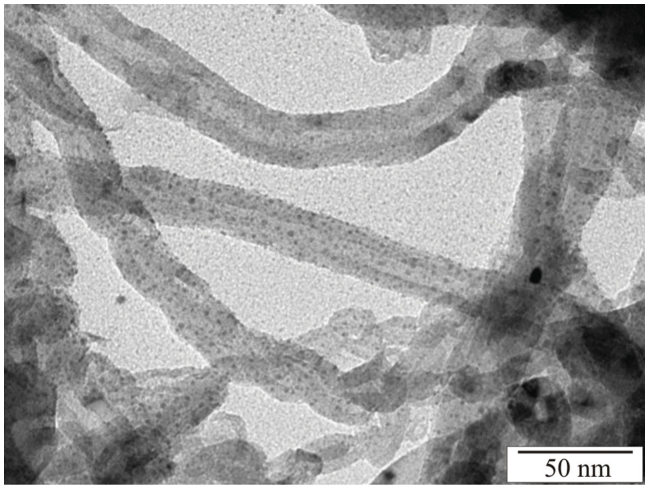

Figure 3. Typical TEM image of Au-MWCNTs.

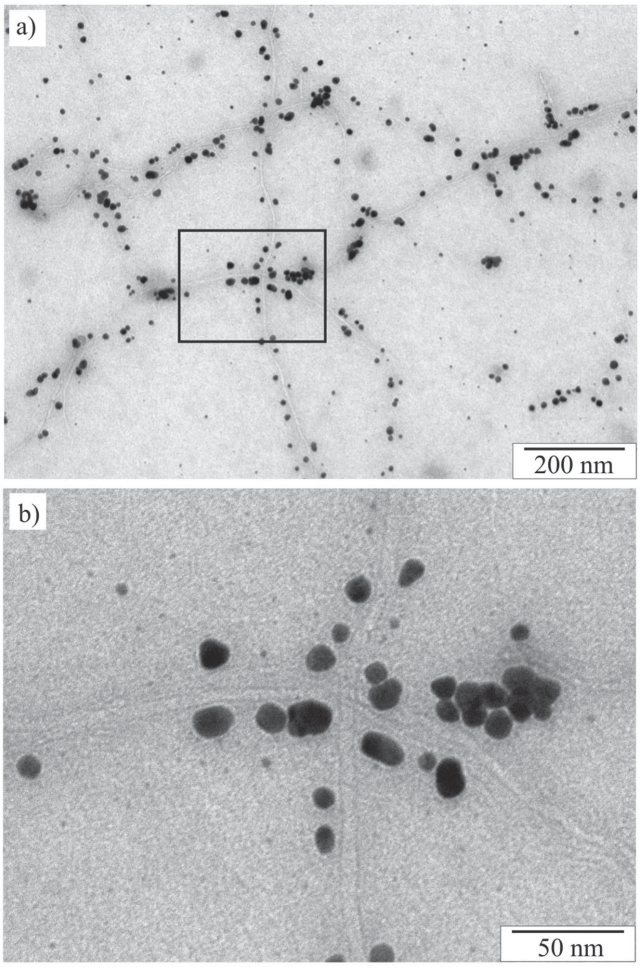

Figure 4. Typical TEM image of: a) cav-Au-MWCNTs and b) zoom-in of the selected area.

atomic concentrations ([*N*] = 3% and 2% at. conc.) for the samples treated in the SAM process for 13 and 24 h, curves (3) and (4) respectively, indicating that 13 h is sufficient to fully functionalize the Au-MWCNTs with cavitand **4**.

The resistive sensor consists of a hybrid nanomaterial, which comprises both recognition and transducer elements, embedded in a standard electronic device. With a cavity depth in the order of 8.3 Å, a quinoxaline-bridged cavitand **4** can completely include one BTEX molecule and form a 1:1 host–guest complex mainly stabilized by π–π and CH–π interactions.[23] The Au-MWCNTs are selected as an integral part of the resistive sensor. They provide sites where the thioether groups of the cavitand **4** can be anchored. The oxygen plasma treatment resulted in the presence of oxygenated defects on the outer wall of MWCNTs. Such defects help gripping, nucleating, and stabilizing Au-NPs. Conversely, pristine carbon nanotubes show very weak interactions with the Au-NPs by establishing interactions with the p-orbitals of the sp^2 carbons of the network.[24] Theoretical studies have shown that Au atoms get trapped at VO_2 defects (oxygenated vacancies), which are the most abundant in oxygen plasma treated MWCNTs compared to V_2O_2 defects (oxygenated di-vacancies), with a binding energy that is 0.55 eV higher than the binding energy of Au-decorated pristine MWCNT.[25] DFT calculations indicated that the presence of oxygen atoms at the functionalized site reduces the HOMO (highest occupied molecular orbitals)–LUMO (lowest unoccupied molecular orbitals) gap to 0.82 eV. This reduction can be explained by the higher density of states near the Fermi level, arising from the overlap of the 2p electrons of the O atoms and the p electron system of the nanotube.[26] MWCNTs can either be metallic or semiconducting depending on the axial chirality of the individual shells and depending on the intershell interaction. A detailed description of their conductance is rather complex, but the main contribution to charge conduction near the Fermi energy level is given by the outer tube. Mats of MWCNTs, such as those employed in the present experiment, consist of a mixture of metallic and semiconducting tubes. Macroscopically, these mats behave as mild p-type semiconductors since their conductance increases or decreases upon adsorption of electron-accepting or donating molecules, respectively.[19b,25] Furthermore, according to DFT calculations, the decoration with Au-NPs slightly perturbs the band structure of MWCNTs causing a small shift of the Fermi level energy toward lower energies, which is equivalent to a p-doping of the tubes (i.e., there is a small electronic charge transfer from the tube to the Au-NP).[27] Finally, since the MWCNT mat consists of defective nanotubes,[28] its resistance is mostly influenced by the resistance of individual nanotubes and not by the internanotube or the electrode–nanotube junctions.[29] Upon formation of the host–guest complex, BTEX⊂cavitand **4** (molecular recognition event), and by assuming the existence of a close proximity between the walls of the cavitand **4** and the surface of the MWCNT, we are prone to speculate that the overall resistance of the MWCNT mat will be influenced (transducer function).

2.3. Gas Sensing Properties

Four cav-Au-MWCNT sensors and two Au-MWCNT sensors were employed for the study of the gas sensing capabilities. Au-MWCNT sensors were fabricated employing the same conditions to those used for cav-Au-MWCNT sensors, but the last step (i.e., the functionalization with cavitand **4** via SAM) was performed just with pure chloroform to induce the aggregation of the Au-NPs on the same level. Each measurement was repeated at least three times. The typical response and recovery cycles of a cav-Au-MWCNT sensor toward increasing concentrations of benzene in dry air are shown in **Figure 6**a. The signal-to-noise ratio for the sensor response was high. The response and recovery cycles were recorded, while the sensor was operated at room temperature and the sensing process was demonstrated to be reversible. During the recovery phase, pure dry air was flown resulting in full baseline resistance recovery. The measurement period lasted for about 6 months in which no significant changes in the baseline resistance nor in sensitivity were observed. In short, the sensor response is reversible and not affected by long-term drift. The typical calibration curves for the cav-Au-MWCNT sensor exposed to benzene, toluene, *o*-xylene, ethanol, and carbon monoxide are depicted in Figure 6b. This sensor showed significantly higher sensitivity to benzene than to the other tested pollutants. At

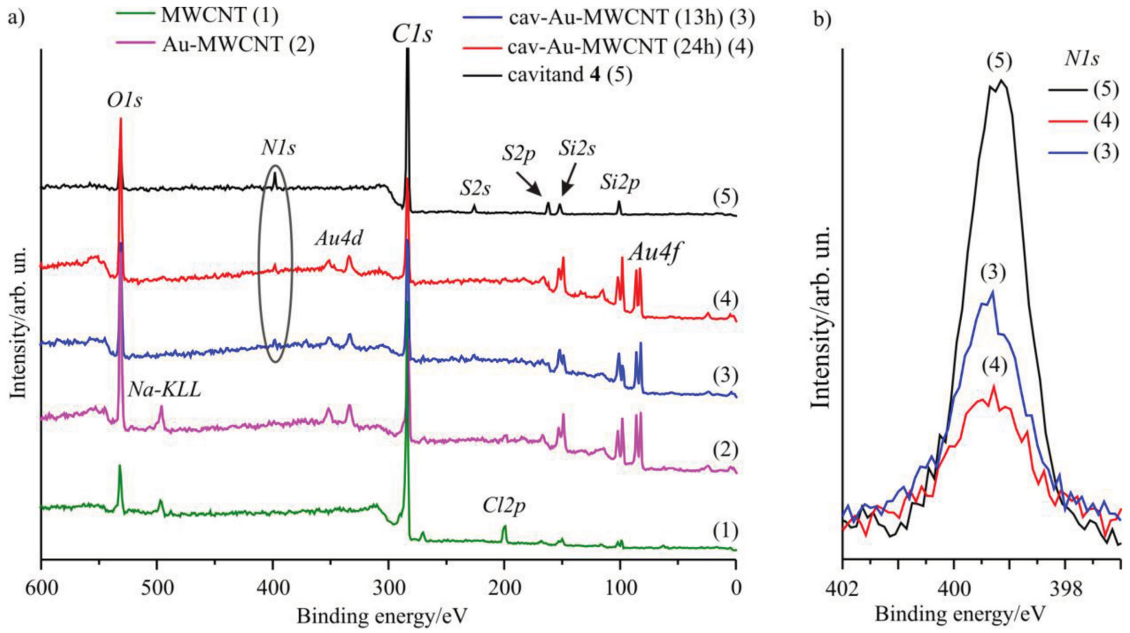

Figure 5. a) Survey spectra acquired for each step of the MWCNTs modification (1–4) and for the cavitand **4** (5). b) A zoom-in of N_{1s} core level spectra is plotted as acquired from cavitand **4** (5) and cav-Au-MWCNT samples (3 and 4).

100 ppb level of benzene, the sensor is seven and 30 times more responsive than to toluene or *o*-xylene, respectively. Furthermore, the slope of the calibration curve (i.e., sensitivity) was calculated for the two lowest tested concentrations and was found to be much higher in the case of benzene (4.2×10^{-3}% ppb^{-1}) than for toluene (1.1×10^{-4}% ppb^{-1}) and *o*-xylene (3.3×10^{-5}% ppb^{-1}). Therefore, the sensor should be able to detect with high sensitivity traces of benzene in the presence of toluene and/or *o*-xylene. The responses to ethanol and carbon monoxide were significantly lower. In summary, the sensor is partially selective toward benzene and a possible strategy for further enhancing selectivity (beyond the scope of this paper) would be to use an array of sensors with different sensitive layers together with a pattern recognition engine.[30] Taken together, these results demonstrated an unprecedented high sensitivity of the cav-Au-MWCNT sensor for benzene. The different species whose sensing is reported in Figure 6b are electron donors. The overall resistance of the cav-Au-MWCNT mat increased when exposed to any of these species. Macroscopically, this implies that our hybrid nanomaterial retains the p-type semiconductor behavior observed for bare or Au-MWCNT mats.

As often encountered in gas sensors, sensitivity and dynamics of response can be further enhanced by increasing the gas flow rate (**Figure 7**a). When the flow is increased, layer gradient that defines a profile of laminar flow attenuated in the boundary layer at the sensor surface. This allowed a better diffusion of benzene toward the sensing layer, and results in an increase in the concentration of the inclusion complexes BTEX⊂cavitand **4** on the surface of MWCNTs mats and therefore a higher sensor response was observed.[31] Up to 2.5 ppb of benzene in air can easily be detected at 400 mL min^{-1} (Figure 7b). To the best of our knowledge, this is the first system that can detect such a low level of benzene in the gas phase by employing a CNT-based material.

Even at very low benzene levels, the response of the sensor was highly reproducible (**Figure 8**). Thanks to the low levels of noise in the response signals, the theoretical LOD for the sensors was calculated to be 600 ppt, which corresponds to a sensor response three times higher than the level of the noise.[32] The responses to benzene provided by the Au-MWCNT sensor were tested for comparison. The Au-MWCNT sensor was not responsive to benzene vapor levels under 60 ppb in dry conditions. Even at this concentration (60 ppb), the response was low. This observation is in good agreement with theoretical findings that predict a very weak binding energy and the lack of charge transfer between the benzene molecule and the Au-MWCNTs system.[27] These results supported the idea that cavitand **4**, in junction with Au-NPs and MWCNTs, was necessary for the high sensitivity measured for benzene.

2.4. Gas Sensing Mechanism

In **Figure 9**, we portray a simplified scheme of the plausible mechanisms for benzene sensing and recovery. We propose that the interior of cavitand **4**, anchored to the surface of cav-Au-MWCNT, is initially occupied by an air molecule (e.g. nitrogen). This status of the system is referred to as N_2⊂cav-Au-MWCNT. The inclusion of guest in the cavity of **4** is a dynamic process allowing a constant chemical exchange between free and included air molecules. When the N_2⊂cav-Au-MWCNT system is exposed to air contaminated with benzene vapors, some of the cavitands bind a benzene molecule. Cavitand **4** shows higher affinity for benzene than nitrogen owing to the establishment of additional interactions (CH–π and π–π) between the benzene and the walls of the cavitand. In solution, the exchange process is referred to as "hostage-exchange mechanism" and occurs via significant conformation changes involving moving from the

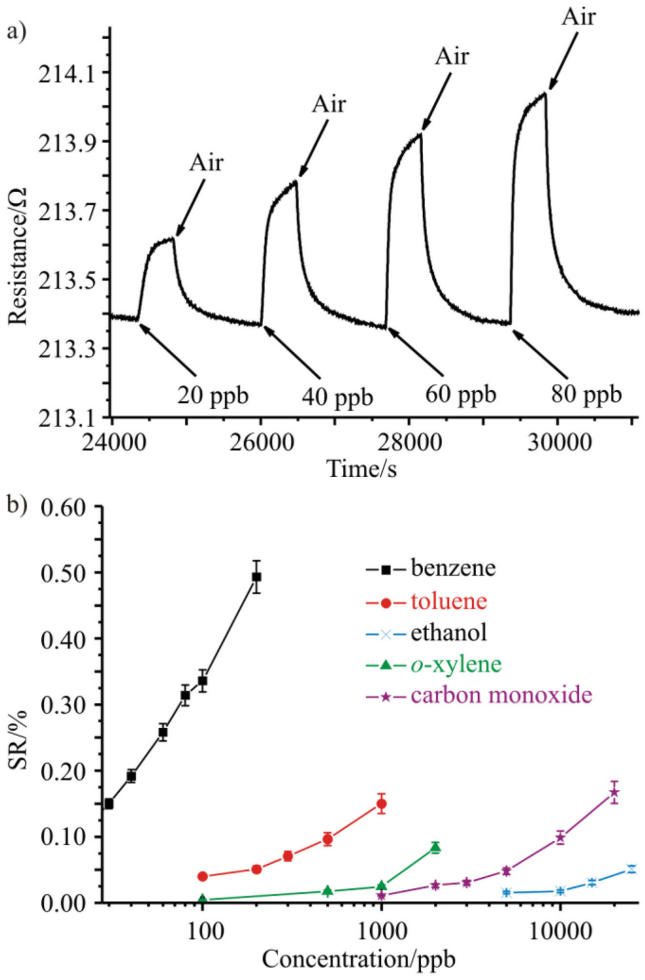

Figure 6. a) A typical cav-Au-MWCNT sensor resistance response in function of benzene concentration in air. b) The relative sensor response for different gas contaminants. In all experiments, we employed a gas flow of 200 mL min^{-1}.

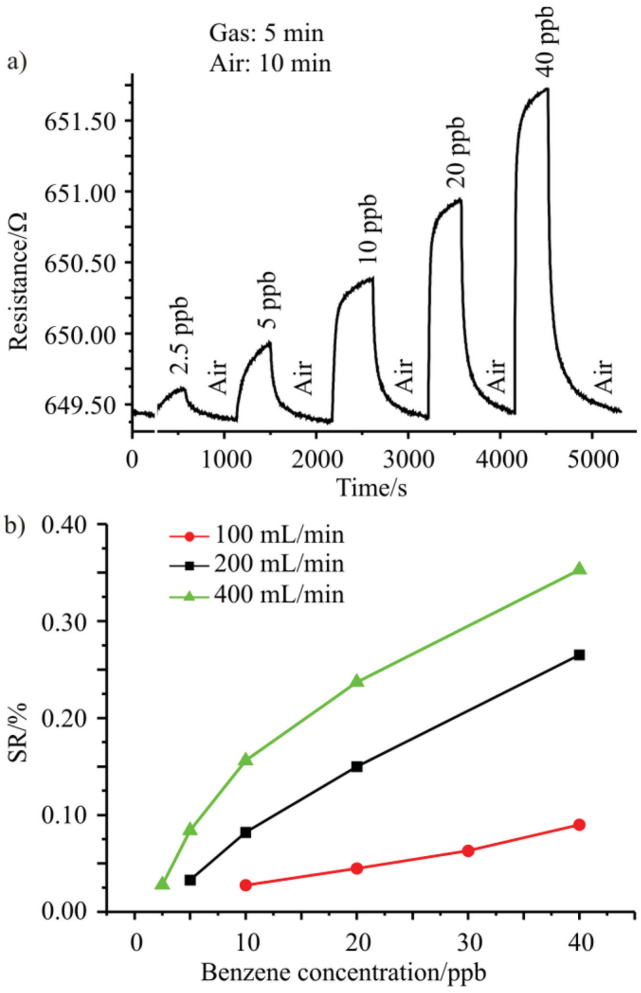

Figure 7. a) cav-Au-MWCNT sensor resistance response in function of benzene concentration in air at 400 mL min^{-1}, and b) the relative sensor response for benzene at different gas flows.

vase to the kite conformation of the cavitand, a process with an energy barrier of 11.6 kcal mol^{-1}.[33] The kite conformation of the N_2⊂cav-Au-MWCNT allows an easy access of a guest molecule (benzene) to the shallow cavity of the cavitand and substitution of the previously bound guest molecule (N_2).[33] Upon guest-exchange, the cavitand's walls fold back to vase conformation producing a new host–guest inclusion complex (referred to as benzene⊂cav-Au-MWCNT). In this way, two inclusion complexes are present on the surface of cav-Au-MWCNT, one with an included nitrogen molecule and the other with a benzene molecule (Figure 9, marked with *).

To explain the transduction mechanism, we hypothesized two plausible types of communications between the cavitand and the MWCNT (**Figure 10**). The first type of communication would involve gold mediation between the π-electron cloud(s) of the quinoxaline wall(s) from the cavitand and the π-electron clouds of MWCNT (referred to as π–Au–π communication). The second type of communication would exclude gold mediation and occur between cavitand molecules located on the edge of Au-NPs whose quinoxaline wall(s) are in direct

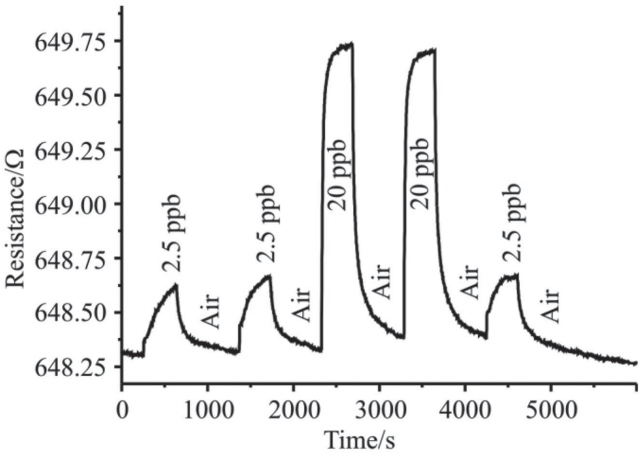

Figure 8. The cav-Au-MWCNT sensor resistance response in function of two benzene concentrations (2.5 and 20 ppb) exposed to sensor in a random order.

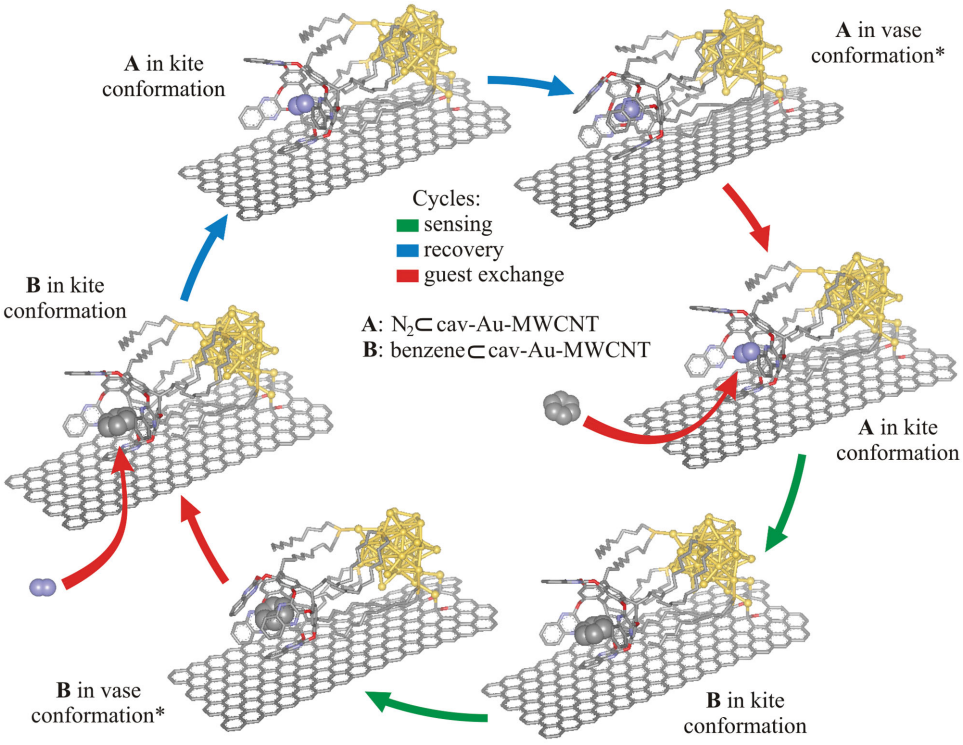

Figure 9. Proposed benzene sensing and recovery mechanism. Benzene and nitrogen molecules are shown as CPK models. Hydrogen atoms are omitted for clarity. Notes: *—crucial structures in the sensing process.

contact with the MWCNT surface allowing π–π stacking interaction (referred to as π–π communication). In both cases, the π-electron density of the quinoxaline walls of the cavitand must be affected by the nature of the included guest molecule (benzene or air molecule). Upon inclusion of a benzene molecule, which also possesses delocalized π-electrons, additional π–π interactions can be established between benzene and the cavitand wall. As a consequence, the π-electron density of the cavitand walls is modified. These electron density changes are translated onto the π-electron clouds of the MWCNT through a charge-transfer/electron-transfer mechanism. This results in hole depletion and decrease in the conductance of MWCNT, experimentally measured as an increase in sensor resistance. Conversely, the stream of pure air modifies the equilibria between benzene⊂cav-Au-MWCNT and N_2⊂cav-Au-MWCNT. The formation of the latter inclusion complex recovers the initial state of the sensor and therefore the baseline resistance of the sensor.

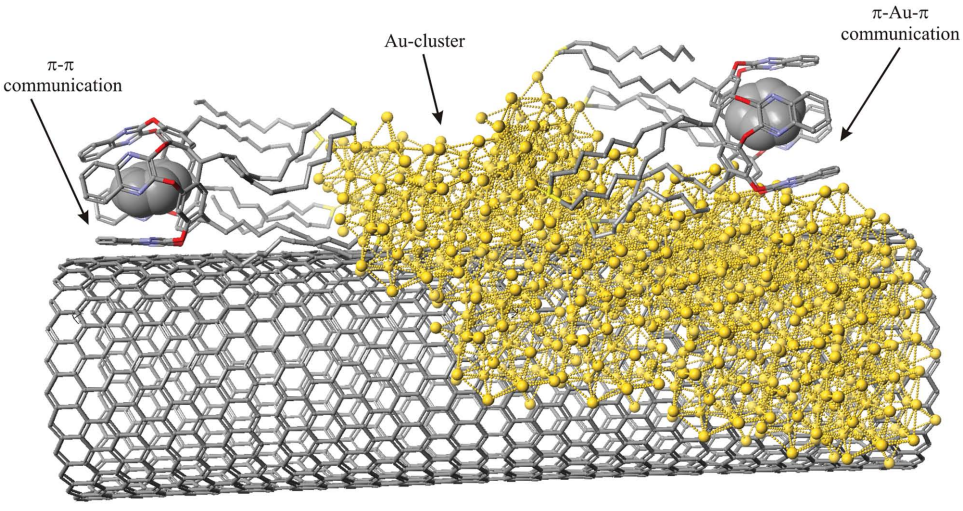

Figure 10. Representation of two proposed types of communications between the cavitand **4** and the Au-MWCNT. Benzene molecules are presented as CPK models. Hydrogen atoms are omitted for clarity.

The lower response displayed by the sensor (reduced increase in resistance) toward the more electron-rich toluene and *o*-xylene molecules, which based on the sensing mechanism proposed above, must imply a reduction of the electron-donating capabilities of their inclusion complexes with the cavitand **4**, is not clear to us. On the one hand, published binding experiments demonstrated that toluene and *o*-xylene, in fact, bind more strongly than benzene inside the cavitand **4** in both the liquid and gas phase.[15a,23] On the other hand, the dipole moments of benzene, toluene, and *o*-xylene are 0, 0.36, and 0.64 D, respectively. We speculate that the lack of dipole moment exhibited by benzene could be somehow responsible for the different electron donating properties assigned to its host–guest complex (benzene⊂cav-Au-MWCNT). Clearly, the verification of this hypothesis must await the results of further experimental and theoretical studies that are beyond the scope of the present work.

Nitrogen dioxide gas belongs to the so-called NO_x and is a toxic gas released from combustion facilities and automobiles.[34] Thus, it is present in atmosphere and its effect has to be studied on our sensors. The adsorption of NO_2 was reported to occur either over Au-NP or over oxygenated defects and exhibits strong response.[27,35] The first-principle modeling of gas adsorption on Au-MWCNT revealed that NO_2, a polar molecule with partial positive charge localized on the nitrogen atom and partial negative charge delocalized among oxygen atoms, is attracted to Au-NPs by its nitrogen atom. The computed binding energies and bond lengths showed that NO_2 strongly interacts with Au-NPs and that the molecule accepted a significant amount of electronic charge from the Au-MWCNT system. This hypothesis is consistent with the well-known electron accepting nature of this molecule.[27] Quantum electron transport calculations revealed that the adsorption of a single NO_2 molecule on the surface of the Au-NP resulted in a remarkable decrease of the Fermi energy level of the Au-MWCNT system.[27] This is consistent with the decrease in resistance that we observed for Au-MWCNT mats in the presence of NO_2.

The response of both cav-Au-MWCNT and Au-MWCNT sensors to different concentrations of NO_2 was also studied. The calibration curve of NO_2 detection for a cav-Au-MWCNT and Au-MWCNT sensors operated at room temperature can be found in the Supporting Information. The response toward NO_2 displayed by cav-Au-MWCNT sensor is about two times lower than that exhibited by the Au-MWCNT sensor. However, NO_2 cross-sensitivity of cavitand-functionalized sensors remains noticeable. The cav-Au-MWCNT may remain somewhat responsive to NO_2 because this molecule can be adsorbed directly onto Au-NPs. However, the important decrease in the response toward NO_2 observed for cav-Au-MWCNTs in comparison to that of Au-MWCNTs indicated that the presence of the cavitand significantly reduced the affinity of Au-NPs to adsorb NO_2 molecules. From a practical point of view, if the detection of benzene should be performed in an environment in which the presence of trace levels of nitrogen dioxide is likely, a detector comprising two sensors, namely one cav-Au-MWCNT sensor and one Au-MWCNT sensor, could be used for benzene level correction. Further details on this strategy are given in the Supporting Information.

Ambient moisture plays an important role in the response of chemiresistors.[36] Therefore, a new set of measurements was performed in which trace concentrations of benzene, toluene, or *o*-xylene in a flow of dry synthetic air were humidified to 10%, 25%, and 60% of relative humidity (R.H.). Taking into account that the pressure was 1 atm and the temperature was 22 °C, the relative humidity tested corresponds to levels that ranged between 2630 and 15 980 ppm of water, i.e., three to five orders of magnitude higher than the concentrations of the aromatic VOCs present in the mixtures. The presence of moisture affected the sensitivity of the cavitand-Au-MWCNT sensor toward VOCs. Response and recovery cycles for benzene under humid conditions together with calibration curves can be found in the Supporting Information. According to these results, the sensitivity of the sensor toward benzene (i.e., slope of the calibration curve) is 4.20% ppm^{-1} under dry conditions and changed to 1.41% ppm^{-1} at 10% R.H., 0.48% ppm^{-1} at 25% R.H., and 0.45% ppm^{-1} at 60% R.H. Taken together, these results indicated that the presence of moisture affected significantly the limit of detection (LOD) of the sensor for benzene. While the benzene LOD remains below 20 ppb for R.H. up to 25%, it rises to about 50 ppb at 60% R.H. In case of toluene or *o*-xylene, the presence of moisture resulted in the cav-Au-MWCNT sensor not displaying any measurable response for both aromatic VOCs up to at concentrations of 5000 ppb (i.e., the partial selectivity is not destroyed by the presence of humidity). Two possible strategies can be exploited to overcome the loss in benzene sensitivity caused by ambient moisture. The first option would involve dehumidification by employing inexpensive filters containing polymers such as polyacrylate, polypyrrole, or sodium polyacrylate salts, which selectively absorb polar compounds (i.e., water) from the input gas flow leaving nonpolar compounds such as benzene unaffected. This strategy has been implemented in solid-phase microextraction for quantitative gas or liquid chromatography analysis of environmental samples[37] or in hand-held photoionization gas.[38] The second option would involve sensor redesign taking into consideration that the oxygen plasma treatment of MWCNTs used to generate defects at their surface for anchoring Au nanoparticles makes CNTs more hydrophilic. Even if the employed cavitand has a hydrophobic character, oxygenated defects present on the surface of carbon nanotubes can be responsible for sensor moisture cross-sensitivity. Alternative methods for achieving Au decoration of CNT sidewalls have been reported, which accounts on the hydrophobic nature of pristine, nondefective CNTs[39] which could be taken into advantage for reducing effect of ambient moisture to the sensor's response.[40]

3. Conclusion

In conclusion, a simple technique for functionalizing the multiwall carbon nanotubes, in view of designing a gas sensor with a superior performance, has been introduced. A quinoxaline-walled thioether-legged cavitand **4** is attached onto oxygen plasma treated Au-NP decorated MWCNTs. The technique is suitable for the mass production of described hybrid sensing nanomaterial at low production costs, allowing cost-effective commercialization. The cavitand-functionalized MWCNT sensor shows unprecedented high sensitivity toward low levels of benzene in dry air at trace levels. The detection of 2.5 ppb is

demonstrated experimentally and a theoretical LOD of 600 ppt was calculated. Furthermore, sensor response toward toluene and *o*-xylene is significantly lower, clearly showing the strong response for benzene, which is the first example of such selective carbon nanotube-based material. This was possible thanks to the molecular recognition introduced by quinoxaline-bridged cavitand **4**. The sensor shows significant cross-sensitivity to NO_2, but this can be compensated by combining a cav-Au-MWCNT sensor with an Au-MWCNT sensor, since the latter is more sensitive to NO_2 and while insensitive to benzene levels below 60 ppb. The cav-Au-MWCNT sensor response toward aromatic VOCs diminishes as the relative humidity in the gas flow increases. It remains responsive to benzene traces in the presence of humidity, but it becomes insensitive to toluene or *o*-xylene in the same range of concentrations. Possibilities of avoiding the effect of moisture could be the dehumidification of the gas flow by employing a inexpensive filter, or keep the hydrophobic character of MWCNTs by using an alternative route to the oxygen plasma treatment used to anchor gold nanoparticles. Finally, it is worth mentioning that both the detection and the recovery of the baseline are performed at room temperature, which implies that these sensors can operate at very low power consumption. This makes the sensor suitable for being integrated in hand-held portable analyzers, wearable detectors, and semipassive radio frequency identification tags with sensing capabilities or in the nodes of wireless sensor networks with a wide range of potential applications in environmental monitoring, workplace safety, or medical devices, among others.

4. Experimental Section

The cavitand **4** was synthesized following a reported procedure.[9c,10a] The synthesis of **4** was accomplished in four steps: 1) acid-catalyzed condensation of 10-undecenal with resorcinol to yield the resorcin[4]arene framework **1**; 2) TMS protection of the OH groups in the upper rim of the resorcin[4]arene to afford cavitand **2**; 3) addition of 1-decanethiol to the terminal alkenes of the legs of cavitand **2** with concomitant cleavage of the TMS-protecting groups afforded cavitand **3**; finally, 4) base promoted coupling of **3** with 2,3-dichloroquinoxaline produced cavitand **4** (details on the synthesis are reported in the Supporting Information).

The chemical compositions of O-MWCNT, Au-MWCNT, and cav-Au-MWCNT samples were analyzed using X-ray photoelectron spectroscopy (XPS), VERSAPROBE PHI 5000 from Physical Electronics, equipped with a Monochromatic Al Kα X-ray. The energy resolution was 0.7 eV. For the compensation of built-up charge on the sample surface during the measurements, a dual beam charge neutralization composed of an electron gun (≈1 eV) and the argon ion gun (≤10 eV) were used.

MWCNTs were obtained from Nanocyl (3101 grade). They were grown by chemical vapor deposition with purity higher than 95%. Carbon nanotubes were up to 1.5 µm long and 9.5 nm in outer diameter. They underwent an oxygen plasma treatment to clean them from amorphous carbon, to promote their dispersion in an appropriate solvent, and to create reactive sites (i.e. oxygenated vacancies, O-MWCNTs) in which metal nanoparticles can nucleate. O-MWCNTs were suspended in chloroform (0.5% w/w) and sonicated during 30 min to uniformly disperse them in the solution, which led to a reproducible CNT density. The prepared suspension was air-brushed on an alumina substrate that comprised 10 × 10 mm screen-printed, Pt-interdigitated electrodes with gap of 500 µm between electrodes. During the airbrushing, the substrate was kept at 100 °C for achieving fast evaporation of the solvent coupled with the resistance monitoring of the device until it reached the defined value of 5 kΩ. This strategy, which is very similar to the one reported by Zilberman et al.,[41] enables us to control both the density of the CNT coating and the amount of O-MWCNTs deposited, ensuring device-to-device reproducibility. To ensure the complete removal of the solvent and promote adhesion of the MWCNT mat to the substrate, sensors were heated at 150 °C for 2 h. The final resistance of thermally treated sensors was a few hundred of ohms.

The next step was decoration of O-MWCNTs with Au-NPs achieved by the RF sputtering process conducted at 13.56 MHz with a power of 30 W under Ar plasma at room temperature, under 0.1 Torr, for 10 s. For the formation of the self-assembled monolayer of the deep cavitand, sensor substrates were immersed in a solution (20 mL) of the cavitand (0.5×10^{-3} M). The SAM process was conducted at 60 °C for a period of maximum 24 h. These conditions allowed a reversible adsorption in order to have well-ordered assembly of the quinoxaline-walled cavitand **4**.[8a] Finally, the sensor substrates were cooled to room temperature, rinsed with pure chloroform and dried at 50 °C during 30 min.

The gas sensing properties of the sensors were measured using a miniaturized Teflon chamber (35 mL). Computer-controlled mass flow meters (Bronkhorst hi-tech 7.03.241) and calibrated gas bottles were used (NO_2, CO, ethanol, benzene, toluene, *o*-xylene all diluted in pure air from Praxair), and pure air from Air Products was used to obtain different concentrations. A continuous flow (100, 200, or 400 mL min^{-1}) was used throughout measurements. The flow was humidified to 10%, 25%, and 60% R.H. by employing an Environics Series 4000 gas mixing system (Environics, Inc., Tolland, CT, USA). Once sensors were placed inside the test chamber, they were connected to a multimeter interface, which allowed the real-time reading of the resistance. Sensor response is defined as $SR\% = (R_{gas} - R_{air}) \times 100/R_{air}$. Throughout the whole testing period sensors were always operated at room temperature (25 °C). Given the low concentration levels tested, the measurement rig was checked to rule out the presence of contamination in mass flows and tubing by performing a set of control GC/MS tests (run before, during, and after gas measurements).

Supporting Information

Supporting Information is available online from the Wiley Online Library or from the author.

Acknowledgements

P.C. gratefully acknowledges a Ph.D. fellowship grant from the Universitat Rovira i Virgili. E.L. was supported by the Catalan Institution for Research and Advanced Studies via the ICREA Academia Award and Generalitat de Catalunya (2014 SGR 1267). P.B. and S.K. thank Gobierno de España MINECO (CTQ2011-23014) and Severo Ochoa Excellence Accreditation 2014–2018 (SEV-2013-031), Generalitat de Catalunya (2014 SGR 320), and the ICIQ Foundation for funding. C.B. is a research associate and C. Struzzi is a research fellow at the National Funds for Scientific Research (FRS-FNRS, Belgium). This work was funded in part by NATO under the Science for Peace and Security Program via Grant No. SPS 984511, FNRS-FRFC Contract No. 2.4577.11 "Chemographene" and by the European Science Foundation via grant COST TD-1105 "EuNetAir."

Received: March 27, 2015
Revised: May 5, 2015
Published online: May 29, 2015

[1] a) United States Environmental Protection Agency, Drinking Water Contaminants, http://water.epa.gov/drink/contaminants/index.cfm#Organic (accessed: May 2009); b) European Commission, Air

Quality Standards, http://ec.europa.eu/environment/air/quality/standards.htm (accessed: February 16, 2015).
[2] a) R. Baan, Y. Grosse, K. Straif, B. Secretan, F. El Ghissassi, V. Bouvard, L. Benbrahim-Tallaa, N. Guha, C. Freeman, L. Galichet, *Lancet Oncol.* **2009**, *10*, 1143; b) A. Fassò, G. Arduino, Environmental regulation in the European Union, *Environ. Encyclopedia of Environmetrics*, *2*, Wiley **2012**; c) D. Dougherty, S. Garte, A. Barchowsky, J. Zmuda, E. Taioli, *Toxicol. Lett.* **2008**, *182*, 7; d) R. E. Hester, R. M. Harrison, Volatile Organic Compounds in the Atmosphere, *R. Soc. Chem.* **1995**; e) A. P. DeCaprio, *CRC Criti. Rev. Toxicol.* **1999**, *29*, 283.
[3] The National Institute for Occupational Safety and Health, NIOSH pocket guide for chemical hazards: benzene, www.cdc.gov/niosh/npg/npgd0049.html (accessed: April 4, 2011).
[4] Official Journal of the European Union, 50/EC of the European Parliament and of the Council of 21 May 2008 on ambient air quality and cleaner air for Europe, http://ec.europa.eu/environment/air/quality/legislation/existing_leg.htm (accessed: April 14, 2008).
[5] a) J. Sun, F. Guan, D. Cui, X. Chen, L. Zhang, J. Chen, *Sens. Actuators B: Chem.* **2013**, *188*, 513; b) C. Liaud, N. Nguyen, R. Nasreddine, S. Le Calvé, *Talanta* **2014**, *127*, 33; c) R.-S. Jian, Y.-S. Huang, S.-L. Lai, L.-Y. Sung, C.-J. Lu, *Microchem. J.* **2013**, *108*, 161.
[6] D. J. Cram, S. Karbach, H. E. Kim, C. B. Knobler, E. F. Maverick, J. L. Ericson, R. C. Helgeson, *J. Am. Chem. Soc.* **1988**, *110*, 2229.
[7] a) M. Vincenti, E. Dalcanale, P. Soncini, G. Guglielmetti, *J. Am. Chem. Soc.* **1990**, *112*, 445; b) M. Vincenti, E. Dalcanale, *J. Chem. Soc., Perkin Trans.* **1995**, *2*, 1069.
[8] a) E. U. Thoden van Velzen, J. F. Engbersen, D. N. Reinhoudt, *J. Am. Chem. Soc.* **1994**, *116*, 3597; b) E. U. Thoden van Velzen, J. F. Engbersen, P. J. de Lange, J. W. Mahy, D. N. Reinhoudt, *J. Am. Chem. Soc.* **1995**, *117*, 6853; c) E. U. Thoden van Velzen, J. F. Engbersen, D. N. Reinhoudt, *Synthesis* **1995**, *1995*, 989.
[9] a) F. Dickert, R. Sikorski, *Mater. Sci. Eng.: C* **1999**, *10*, 39; b) Y. Yamakoshi, R. R. Schlittler, J. K. Gimzewski, F. Diederich, *J. Mater. Chem.* **2001**, *11*, 2895; c) V. A. Azov, P. J. Skinner, Y. Yamakoshi, P. Seiler, V. Gramlich, F. Diederich, *Helv. Chim. Acta* **2003**, *86*, 3648.
[10] a) E. B. Feresenbet, M. Busi, F. Ugozzoli, E. Dalcanale, D. K. Shenoy, *Sens. Lett.* **2004**, *2*, 186; b) R. Capan, Z. Özbek, H. Göktaş, S. Şen, F. Ince, M. Özel, G. Stanciu, F. Davis, *Sens. Actuators B: Chem.* **2010**, *148*, 358; c) M. Erdoğan, R. Capan, F. Davis, *Sens. Actuators B: Chem.* **2010**, *145*, 66; d) Y. Liu, T. Taira, M. C. Young, D. Ajami, J. Rebek Jr, Q. Cheng, R. J. Hooley, *Langmuir* **2011**, *28*, 1391; e) A. Hassan, A. Ray, A. Nabok, F. Davis, *Sens. Actuators B: Chem.* **2001**, *77*, 638; f) E. B. Feresenbet, E. Dalcanale, C. Dulcey, D. K. Shenoy, *Sens. Actuators B: Chem.* **2004**, *97*, 211.
[11] O. B. Berryman, A. C. Sather, J. Rebek Jr., *Org. Lett.* **2011**, *13*, 5232.
[12] a) T. Weiss, K. Schierbaum, U. T. van Velzen, D. Reinhoudt, W. Göpel, *Sens. Actuators B: Chem.* **1995**, *26*, 203; b) J. Hartmann, J. Auge, R. Lucklum, S. Rösler, P. Hauptmann, B. Adler, E. Dalcanale, *Sens. Actuators B: Chem.* **1996**, *34*, 305; c) J. Hartmann, P. Hauptmann, S. Levi, E. Dalcanale, *Sens. Actuators B: Chem.* **1996**, *35*, 154; d) R. Paolesse, C. Di Natale, S. Nardis, A. Macagnano, A. D'Amico, R. Pinalli, E. Dalcanale, *Chem. A Eur. J.* **2003**, *9*, 5388; e) O. Mermer, S. Okur, F. Siimer, C. Ozbek, S. Sayin, M. Yilmaz, *Acta Phys. Pol. A Gen. Phys.* **2012**, *121*, 240.
[13] M. Ferrari, V. Ferrari, D. Marioli, A. Taroni, M. Suman, E. Dalcanale, *Sens. Actuators B: Chem.* **2004**, *103*, 240.
[14] a) F. Bianchi, A. Bedini, N. Riboni, R. Pinalli, A. Gregori, L. M. Sidisky, E. Dalcanale, M. Careri, *Anal. Chem.* **2014**, *86*, 10646; b) R. Pinalli, T. Barboza, F. Bianchi, C. Massera, F. Ugozzoli, E. Dalcanale, *Supramol. Chem.* **2013**, *25*, 682.
[15] a) F. Bianchi, R. Pinalli, F. Ugozzoli, S. Spera, M. Careri, E. Dalcanale, *New J. Chem.* **2003**, *27*, 502; b) S. Zampolli, I. Elmi, F. Mancarella, P. Betti, E. Dalcanale, G. Cardinali, M. Severi, *Sens. Actuators B: Chem.* **2009**, *141*, 322; c) S. Zampolli, P. Betti, I. Elmi, E. Dalcanale, *Chem. Commun.* **2007**, *27*, 2790; d) F. Bianchi, M. Mattarozzi, P. Betti, F. Bisceglie, M. Careri, A. Mangia, L. Sidisky, S. Ongarato, E. Dalcanale, *Anal. Chem.* **2008**, *80*, 6423.
[16] a) M. Dionisio, J. M. Schnorr, V. K. Michaelis, R. G. Griffin, T. M. Swager, E. Dalcanale, *J. Am. Chem. Soc.* **2012**, *134*, 6540; b) F. Wang, T. M. Swager, *J. Am. Chem. Soc.* **2011**, *133*, 11181; c) L. Kong, J. Wang, F. Meng, X. Chen, Z. Jin, M. Li, J. Liu, X.-J. Huang, *J. Mater. Chem.* **2011**, *21*, 11109.
[17] J. M. Schnorr, D. van der Zwaag, J. J. Walish, Y. Weizmann, T. M. Swager, *Adv. Funct. Mater.* **2013**, *23*, 5285.
[18] E. Llobet, *Sens. Actuators B: Chem.* **2013**, *179*, 32.
[19] a) P. Clément, I. Hafaiedh, E. Parra, A. Thamri, J. Guillot, A. Abdelghani, E. Llobet, *Carbon* **2014**, *78*, 510; b) R. Leghrib, A. Felten, F. Demoisson, F. Reniers, J.-J. Pireaux, E. Llobet, *Carbon* **2010**, *48*, 3477.
[20] R. Leghrib, E. Llobet, *Anal. Chim. Acta* **2011**, *708*, 19.
[21] I. Suarez-Martinez, C. Bittencourt, X. Ke, A. Felten, J. Pireaux, J. Ghijsen, W. Drube, G. Van Tendeloo, C. Ewels, *Carbon* **2009**, *47*, 1549.
[22] D. J. Cram, M. E. Tanner, C. B. Knobler, *J. Am. Chem. Soc.* **1991**, *113*, 7717.
[23] P. Soncini, S. Bonsignore, E. Dalcanale, F. Ugozzoli, *J. Org. Chem.* **1992**, *57*, 4608.
[24] Y. Zhang, N. W. Franklin, R. J. Chen, H. Dai, *Chem. Phys. Lett.* **2000**, *331*, 35.
[25] J.-C. Charlier, L. Arnaud, I. Avilov, M. Delgado, F. Demoisson, E. Espinosa, C. P. Ewels, A. Felten, J. Guillot, R. Ionescu, *Nanotechnology* **2009**, *20*, 375501.
[26] T. Prasomsri, D. Shi, D. E. Resasco, *Chem. Phys. Lett.* **2010**, *497*, 103.
[27] Z. Zanolli, R. Leghrib, A. Felten, J.-J. Pireaux, E. Llobet, J.-C. Charlier, *ACS Nano* **2011**, *5*, 4592.
[28] J.-C. Charlier, *Acc. Chem. Res.* **2002**, *35*, 1063.
[29] A. Salehi-Khojin, F. Khalili-Araghi, M. A. Kuroda, K. Y. Lin, J.-P. Leburton, R. I. Masel, *ACS Nano* **2010**, *5*, 153.
[30] a) B. Wang, J. C. Cancilla, J. S. Torrecilla, H. Haick, *Nano Lett.* **2014**, *14*, 933; b) G. Konvalina, H. Haick, *Acc. Chem. Res.* **2013**, *47*, 66.
[31] S. Kline, W. Reynolds, F. Schraub, P. Runstadler, *J. Fluid Mech.* **1967**, *30*, 741.
[32] D. MacDougall, W. B. Crummett, *Anal. Chem.* **1980**, *52*, 2242.
[33] a) D. M. Rudkevich, G. Hilmersson, J. Rebek, *J. Am. Chem. Soc.* **1998**, *120*, 12216; b) D. M. Rudkevich, G. Hilmersson, J. Rebek, *J. Am. Chem. Soc.* **1997**, *119*, 9911; c) P. J. Skinner, A. G. Cheetham, A. Beeby, V. Gramlich, F. Diederich, *Helv. Chim. Acta* **2001**, *84*, 2146.
[34] United States Environmental Protection Agency, Nitrogen dioxide, http://www.epa.gov/air/nitrogenoxides/ (accessed: February 30, 2015).
[35] J. Li, Y. Lu, Q. Ye, M. Cinke, J. Han, M. Meyyappan, *Nano Lett.* **2003**, *3*, 929.
[36] K. Balasubramanian, K. Kern, *Adv. Mater.* **2014**, *26*, 1154.
[37] J. Pawliszyn, *Handbook of Solid State Microextraction*, Elsevier, London, UK **2012**.
[38] Humidity filtering tubes for PID detectors, http://www.rae.nl/files/pdf/FeedsEnclosure-Humidity_Tube_II_LR_051507.pdf (accessed: April 30, 2015).
[39] T. Sainsbury, T. Ikuno, D. Okawa, D. Pacile, J. M. Frechet, A. Zettl, *J. Phys. Chem. C* **2007**, *111*, 12992.
[40] X. Guo, *Adv. Mater.* **2013**, *25*, 3397.
[41] Y. Zilberman, U. Tisch, G. Shuster, W. Pisula, X. Feng, K. Müllen, H. Haick, *Adv. Mater.* **2010**, *22*, 4317.